

Measurement of the Differential Cross Section for the Reaction $\gamma n \rightarrow \pi^- p$ from Deuterium

W. Chen,¹ T. Mibe,² D. Dutta,³ H. Gao,¹ J. M. Laget,^{7,4} M. Mirazita,⁵ P. Rossi,⁵ S. Stepanyan,⁴ I. I. Strakovsky,⁶ M. J. Amarian,²⁷ M. Anghinolfi,²⁰ H. Bagdasaryan,^{27,*} M. Battaglieri,²⁰ M. Bellis,¹⁰ B. L. Berman,⁶ A. S. Biselli,^{15,29} C. Bookwalter,¹⁷ D. Branford,¹⁴ W. J. Briscoe,⁶ W. K. Brooks,^{34,4} V. D. Burkert,⁴ S. L. Careccia,²⁷ D. S. Carman,⁴ L. Casey,¹¹ P. L. Cole,^{19,4} P. Collins,⁸ V. Crede,¹⁷ A. Daniel,² N. Dashyan,³⁷ R. De Vita,²⁰ E. De Sanctis,⁵ A. Deur,⁴ S. Dhamija,¹⁶ R. Dickson,¹⁰ C. Djalali,³² G. E. Dodge,²⁷ D. Doughty,^{12,4} H. Egiyan,^{25,36} P. Eugenio,¹⁷ G. Fedotov,³¹ A. Fradi,²¹ M. Garçon,⁷ G. P. Gilfoyle,³⁰ K. L. Giovanetti,²³ F. X. Girod,^{7,†} W. Gohn,¹³ R. W. Gothe,³² K. A. Griffioen,³⁶ M. Guidal,²¹ H. Hakobyan,^{34,37} C. Hanretty,¹⁷ N. Hassall,¹⁸ D. Heddle,^{12,4} K. Hicks,² M. Holtrop,²⁵ C. E. Hyde,^{27,28} Y. Ilieva,³² D. G. Ireland,¹⁸ B. S. Ishkhanov,³¹ E. L. Isupov,³¹ H. S. Jo,²¹ J. R. Johnstone,¹⁸ K. Joo,^{13,35} D. Keller,² M. Khandaker,²⁶ P. Khetarpal,²⁹ W. Kim,²⁴ A. Klein,²⁷ F. J. Klein,^{11,4} L. H. Kramer,^{16,4} V. Kubarovskiy,⁴ S. E. Kuhn,²⁷ S. V. Kuleshov,²² V. Kuznetsov,²⁴ K. Livingston,¹⁸ H. Y. Lu,³² N. Markov,¹³ M. E. McCracken,¹⁰ B. McKinnon,¹⁸ C. A. Meyer,¹⁰ T. Mineeva,¹³ V. Mokeev,^{31,4} B. Moreno,²¹ K. Moriya,¹⁰ P. Nadel-Turonski,¹¹ R. Nasseripour,^{32,‡} S. Niccolai,²¹ I. Niculescu,^{23,6} M. R. Niroula,²⁷ M. Osipenko,^{20,31} A. I. Ostrovidov,¹⁷ K. Park,^{32,24} S. Park,¹⁷ S. Anefalos Pereira,⁵ O. Pogorelko,²² S. Pozdniakov,²² J. W. Price,⁹ S. Proceur,⁷ D. Protopopescu,¹⁸ B. A. Raue,^{16,4} G. Ricco,²⁰ M. Ripani,²⁰ B. G. Ritchie,⁸ G. Rosner,¹⁸ F. Sabatié,^{7,27} M. S. Saini,¹⁷ J. Salamanca,¹⁹ C. Salgado,²⁶ R. A. Schumacher,¹⁰ Y. G. Sharabian,^{4,37} D. I. Sober,¹¹ D. Sokhan,¹⁴ S. S. Stepanyan,²⁴ S. Strauch,³² M. Taiuti,²⁰ D. J. Tedeschi,³² S. Tkachenko,²⁷ M. Ungaro,¹³ M. F. Vineyard,^{33,30} D. P. Watts,^{18,§} L. B. Weinstein,²⁷ D. P. Weygand,⁴ M. H. Wood,³² A. Yegneswaran,⁴ J. Zhang,²⁷ and B. Zhao¹³

(The CLAS Collaboration)

¹Duke University, Durham, North Carolina 27708, USA

²Ohio University, Athens, Ohio 45701, USA

³Mississippi State University, Mississippi State, Mississippi 39762, USA

⁴Thomas Jefferson National Accelerator Facility, Newport News, Virginia 23606, USA

⁵INFN, Laboratori Nazionali di Frascati, 00044 Frascati, Italy

⁶The George Washington University, Washington, D.C. 20052, USA

⁷CEA-Saclay, Service de Physique Nucléaire, 91191 Gif-sur-Yvette, France

⁸Arizona State University, Tempe, Arizona 85287-1504, USA

⁹California State University, Dominguez Hills, Carson, California 90747, USA

¹⁰Carnegie Mellon University, Pittsburgh, Pennsylvania 15213, USA

¹¹Catholic University of America, Washington, D.C. 20064, USA

¹²Christopher Newport University, Newport News, Virginia 23606, USA

¹³University of Connecticut, Storrs, Connecticut 06269, USA

¹⁴Edinburgh University, Edinburgh EH9 3JZ, United Kingdom

¹⁵Fairfield University, Fairfield, Connecticut 06824, USA

¹⁶Florida International University, Miami, Florida 33199, USA

¹⁷Florida State University, Tallahassee, Florida 32306, USA

¹⁸University of Glasgow, Glasgow G12 8QQ, United Kingdom

¹⁹Idaho State University, Pocatello, Idaho 83209, USA

²⁰INFN, Sezione di Genova, 16146 Genova, Italy

²¹Institut de Physique Nucleaire ORSAY, Orsay, France

²²Institute of Theoretical and Experimental Physics, Moscow, 117259, Russia

²³James Madison University, Harrisonburg, Virginia 22807, USA

²⁴Kyungpook National University, Daegu 702-701, Republic of Korea

²⁵University of New Hampshire, Durham, New Hampshire 03824-3568, USA

²⁶Norfolk State University, Norfolk, Virginia 23504, USA

²⁷Old Dominion University, Norfolk, Virginia 23529, USA

²⁸Université Blaise Pascal, Laboratoire de Physique Corpusculaire CNRS/IN2P3 F-63177 Aubière, France

²⁹Rensselaer Polytechnic Institute, Troy, New York 12180-3590, USA

³⁰University of Richmond, Richmond, Virginia 23173, USA

³¹Skobel'syn Nuclear Physics Institute, Skobel'syn Nuclear Physics Institute, 119899 Moscow, Russia

³²University of South Carolina, Columbia, South Carolina 29208, USA

³³Union College, Schenectady, New York 12308, USA

³⁴Universidad Técnica Federico Santa María, Casilla 110-V Valparaíso, Chile

³⁵University of Virginia, Charlottesville, Virginia 22901, USA
³⁶College of William and Mary, Williamsburg, Virginia 23187-8795, USA
³⁷Yerevan Physics Institute, 375036 Yerevan, Armenia
(Received 6 March 2009; published 1 July 2009)

We report a measurement of the differential cross section for the $\gamma n \rightarrow \pi^- p$ process from the CLAS detector at Jefferson Laboratory in Hall B for photon energies between 1.0 and 3.5 GeV and pion center-of-mass (c.m.) angles ($\theta_{\text{c.m.}}$) between 50° and 115° . We confirm a previous indication of a broad enhancement around a c.m. energy (\sqrt{s}) of 2.1 GeV at $\theta_{\text{c.m.}} = 90^\circ$ in the scaled differential cross section $s^7 \frac{d\sigma}{dt}$ and a rapid falloff in a center-of-mass energy region of about 400 MeV following the enhancement. Our data show an angular dependence of this enhancement as the suggested scaling region is approached for $\theta_{\text{c.m.}}$ from 70° to 105° .

DOI: 10.1103/PhysRevLett.103.012301

PACS numbers: 25.10.+s, 13.60.Le, 24.85.+p, 25.20.-x

The $\gamma n \rightarrow \pi^- p$, $\gamma p \rightarrow \pi^+ n$, and $\gamma p \rightarrow \pi^0 p$ reactions are fundamental processes that are ideal candidates for the study of the strong interaction. At intermediate energies these processes have been used to study nucleon resonances and the transition from nucleon-meson to quark-gluon degrees of freedom. Recently at Jefferson Laboratory, the differential cross sections on the charged pion photoproduction on hydrogen (proton) and deuterium (deuteron) targets [1,2] have been measured at intermediate energies. These measurements have shown that the differential cross section for pion photoproduction at fixed c.m. angles of 70° and 90° seem to scale as $d\sigma/dt \propto s^{-(n-2)}$ as predicted by the constituent counting rule (CCR) [3,4]. Here s is the invariant Mandelstam variable for the total energy squared, and n is the total number of point particles and gauge fields involved. The CCR was proposed as a signature for the transition from the nucleon-meson to the quark-gluon picture. While such predicted scaling behavior has been seen in a number of exclusive reactions at a specific kinematic regime [5–11], questions remain such as why scaling seems to set in at a surprisingly low transverse momentum value above about 1.1 GeV/c [9,11]. If the observed scaling is the expected CCR, is there a clear signature for such a transition?

In addition to the onset of scaling, the recent charged pion photoproduction experiment [1,2] also observed an apparent enhancement in the scaled differential cross section at $\theta_{\text{c.m.}} = 90^\circ$ and at $\sqrt{s} \approx 1.8\text{--}2.5$ GeV. Furthermore, just before the onset of scaling behavior, the scaled cross section drops by a factor of 4 in a very narrow c.m. energy range of few hundreds of MeV around $\sqrt{s} = 2.5$ GeV. Is this a signature for the transition from the nucleon-meson degrees of freedom to the quark-gluon degrees? The coarse energy binning of these data did not allow for a detailed investigation of either the true nature of the apparent scaling behavior or the observed enhancement, and it did not allow for an analysis of the drop in the differential cross section.

In this Letter, we report on a measurement aimed at a mapping of the transition from one region to another and providing a detailed investigation of the observed enhance-

ment and the drop in the differential cross section for the $\gamma n \rightarrow \pi^- p$ process. This measurement was carried out over the range \sqrt{s} from 1.8 to 2.5 GeV with a very fine photon energy binning and a high statistical precision, using the Jefferson Laboratory CEBAF Large Acceptance Spectrometer (CLAS) [12] in Hall B.

The CLAS instrumentation was designed to provide large coverage of charged particles ($8^\circ \leq \theta \leq 140^\circ$). It is divided into six sectors by six superconducting coils which generate a toroidal magnetic field. Each sector acts as an independent detection system that includes drift chambers (DCs), Cherenkov counters, scintillation counters (SCs), and electromagnetic calorimeters. The drift chambers determine the trajectories of charged particles. With the magnetic field generated by the superconducting coils, the momenta of the charged particle can be determined from the curvature of the trajectories. The scintillation counters measure the time-of-flight and provide charged particle identification when combined with the momentum information from the drift chambers. Details about the CLAS detector can be found in Ref. [12].

A 24-cm-long liquid-deuterium target was employed with the target cell positioned 25 cm upstream from the CLAS nominal center. A tagged-photon beam [13] generated by a 3.8-GeV electron beam incident on a gold radiator with a radiation length of 10^{-4} corresponded to a maximum \sqrt{s} of 2.8 GeV for the process of interest. The event trigger required at least two charged particles in different sectors. Two magnetic field settings were used during the experiment, corresponding to a low-field setting (with toroidal magnet current $I = 2250$ A) for better forward angle coverage, and a high-field setting ($I = 3375$ A) for better momentum resolution. About 10^{10} triggers were collected during a running period of about two months.

The raw data collected from the experiment were first processed to calibrate and convert the information from the detector subsystems to physical variables for detected particles such as energy, momentum, position, and timing information. The events of interest for which the photon coupled to the neutron inside the deuteron were selected by ensuring a proton and a π^- in the final state. The difference

of the reconstructed time of photon and charged particles at the reaction vertex was required to be within 1 ns to ensure that they came from the same accelerator electron bunch, which had a period of 2.004 ns. The momentum of the spectator proton in the deuteron is mostly below 200 MeV/c and is therefore not detected by CLAS. The 4 momentum of the undetected proton was reconstructed by energy-momentum conservation. Only events with missing mass around the proton mass were selected to make sure that the missing particle was the undetected proton. Shown in Fig. 1(a) is a typical reconstructed missing mass squared distribution. A 3σ cut was applied to identify the proton. Monte Carlo simulations for the $\gamma n \rightarrow \pi^- p$ process based on a phase space generator have been carried out to determine the acceptance. In the simulation, the neutron momentum distribution inside the deuteron is based on the deuteron wave function obtained from the Bonn potential [14]. Figure 1(b) shows the reconstructed proton momentum from the experimental data and the simulation. The excellent agreement between the data and the Monte Carlo for a missing momentum below 200 MeV/c justified the cut we used (shown by the dashed line) in our analysis to select the quasifree events of $\gamma n \rightarrow \pi^- p$ from deuterons.

To extract the cross section, the aforementioned phase space based simulation is used to correct for events lost due to geometrical constraints and detector inefficiencies. The response of the CLAS detector was simulated in GEANT. More than 10^8 of events were generated and passed through the simulation. The simulated data were then processed to incorporate the subsystem efficiencies and resolutions extracted from the experiment. The DC wire efficiency and SC efficiency were studied in detail. The “excluded-layer method” [15] was used to study the DC wire efficiency and identify the bad DC regions. The SC efficiency was extracted by studying the SC occupancies.

The correction due to the SC inefficiency is about 20% for the $\gamma n \rightarrow \pi^- p$ channel. All the simulated data were then processed by the same software used in the real data processing and analysis. The ratio between the events that passed the simulation and the generated events is a product of the detector efficiency and the acceptance.

The final state interaction (FSI) effects have been taken into account before one extracts cross sections on the neutron since a deuteron target is used. The FSI correction is calculated according to the Glauber formulation [16], and this correction is about 15%–30%, depending on energy and angle.

The differential cross section in the c.m. frame of the γn system is then given by

$$\frac{d\sigma}{d\Omega_{\text{c.m.}}} = \frac{N}{t_G \epsilon} \frac{1}{N_\gamma} \frac{A}{\rho L N_A} \frac{1}{d\Omega_{\text{c.m.}}}, \quad (1)$$

where t_G is the correction [16] for the FSI, ϵ is the product of the detector efficiency and acceptance, N is the number of events, N_γ is the total number of photons incident on the target, and A , N_A , L , ρ are deuteron atomic mass, Avogadro’s number, target length, and target density, respectively. The scaled differential cross section is defined as

$$s^7 \frac{d\sigma}{dt} = s^7 \frac{d\sigma}{d\Omega_{\text{c.m.}}} \frac{d\Omega_{\text{c.m.}}}{dt} = s^7 \frac{d\sigma}{d\Omega_{\text{c.m.}}} \frac{\pi}{E_{\text{c.m.}}^\gamma p_{\text{c.m.}}^{\pi^-}}, \quad (2)$$

where $E_{\text{c.m.}}^\gamma$ and $p_{\text{c.m.}}^{\pi^-}$ are the photon energy and π^- momentum in the c.m. frame, respectively. The results from the high magnetic field setting are consistent with those from the low magnetic field setting within systematic uncertainties. The results from the two settings are combined.

There are three major sources of systematic uncertainties: the luminosity, the FSI correction, and the background. We studied the target thickness fluctuations as

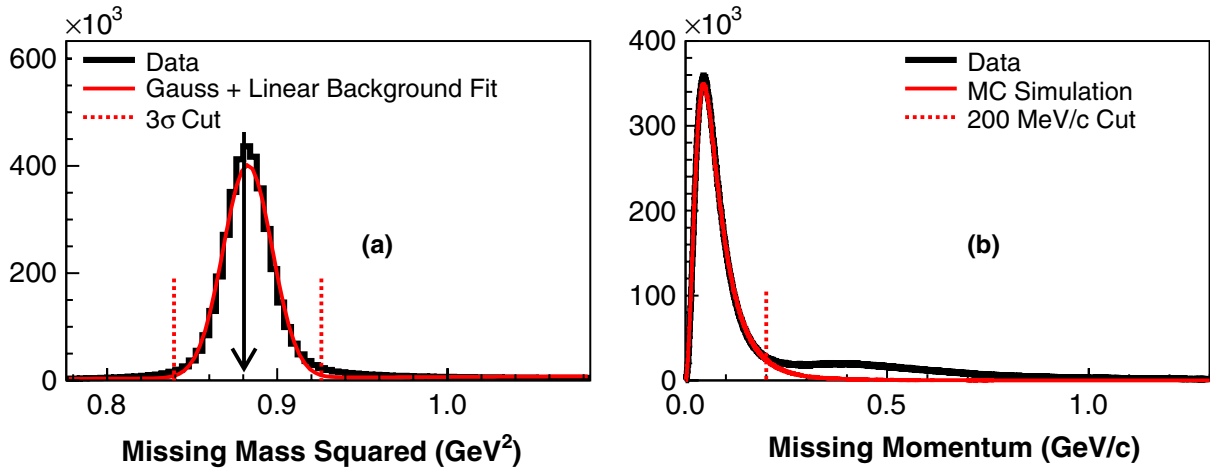


FIG. 1 (color online). (a) Reconstructed missing mass squared of the spectator proton fitted with a Gaussian plus linear function. The arrow indicates the mass squared of the proton. (b) Reconstructed spectator proton momentum (missing momentum) from this experiment together with a Monte Carlo simulation.

seen by the beam, as well as the run-dependent and beam-current-dependent fluctuations of the normalized yield. All of them contribute to the uncertainty in the luminosity, and in total this uncertainty is less than 5%. The uncertainty of the Glauber calculation for the FSI correction was estimated to be 5% in Ref. [1]. To study the model uncertainty in calculating the FSI correction, we carried out another calculation using the approach of Ref. [17]. Both methods agree within 10%. A 10% systematic uncertainty to the differential cross section is assigned for the FSI correction. The background in the missing mass peak region is about 2%–7% depending on the photon energy, and an example is shown in Fig. 1(a). According to Monte Carlo simulations, the background could come from the poorly reconstructed real events due to the DC resolution. Therefore, no background was subtracted in this analysis; instead the fitted background was assigned as the systematic uncertainty. The total systematic uncertainty is the quadratic sum of all the systematic uncertainties, and is between 11% and 13% on the extracted differential cross sections.

Figure 2 shows the scaled differential cross section $s^7 \frac{d\sigma}{dt}$ as a function of \sqrt{s} for $\theta_{c.m.} = 90^\circ$ for three different channels. The results from this experiment are shown in the middle panel as red solid circles with statistical uncertainties, and the systematic uncertainty is shown as a band. The error bars for E94-104 [1] include both the statistical and systematic uncertainties, while only statistical uncertainties are shown for the π^0 data [18] and the π^+ data [19]. All other world data are collected from Refs. [5,20]. Our data are consistent with the E94-104 results [1] within experimental uncertainties. With fine photon energy bins and high statistical precision, our data confirm a broad enhancement around \sqrt{s} of 2.1 GeV in the scaled differential cross section. Our data also confirm a marked falloff of the differential cross section in a narrow energy window of about 400 MeV above this enhancement and the onset of the CCR scaling for \sqrt{s} around 2.8 GeV as suggested by an earlier Jefferson Laboratory experiment [1] (shown as green solid squares). Similar behavior has been seen in the recent CLAS g1c π^+ photoproduction data [19] (magenta open squares in Fig. 2). While this falloff may be taken as a signature for the transition from nucleon-meson degrees of freedom to quark-gluon degrees of freedom, theoretical studies in this region are needed to confirm this speculation. Also shown are the results of the SAID SP09 partial wave analysis [19] (blue solid curve), the MAID07 model [21] (cyan dashed curve), and the prediction from a Regge approach [22] (black solid curve).

In the Regge calculation, no baryon resonances in this energy region were included. And the results did not predict the enhancement seen in our data. Thus the deviation is speculated to be due to baryon resonances [22].

While the SAID SP09 fit has been greatly improved by the CLAS π^0 [18], the π^+ data [19], and the Hall-A π^-

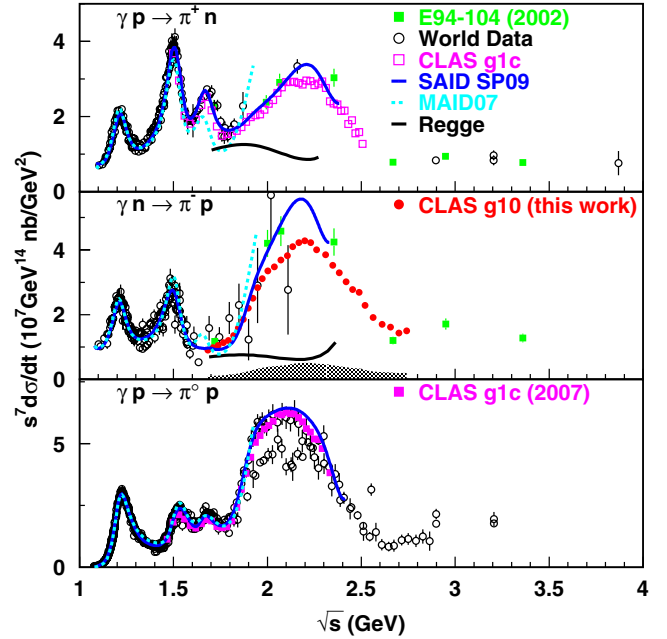


FIG. 2 (color online). Scaled differential cross section $s^7 \frac{d\sigma}{dt}$ as a function of \sqrt{s} for $\theta_{c.m.} = 90^\circ$ for three different channels. The upper panel is for the $\gamma p \rightarrow \pi^+ n$ process, the middle panel is for the $\gamma n \rightarrow \pi^- p$ process, and the lower panel is for the $\gamma p \rightarrow \pi^0 p$ process. The green solid squares are results from Ref. [1], and the results from this experiment are shown as red solid circles. Results from Dugger *et al.* [18] on neutral pion production are shown as magenta solid squares. The magenta open squares are recent CLAS data on π^+ production [19]. The SAID SP09 results [19] are shown as the blue solid curves in all three panels. The prediction from a Regge approach [22] is shown in the top and middle panels by black solid curves. The black open circles are the world data collected from Refs. [5,20].

data [1,2], it does not give as good a description of our data near the peak of the enhancement. Further, it fails to constrain the π^- channel and does not describe our data well above \sqrt{s} of 2.3 GeV (not shown in Fig. 2). The precision data presented here will help to further constrain the SAID fit and will allow for a determination of the corresponding neutron electromagnetic parameters for resonances classified as 4 star by the PDG [23]. These studies will be reported in a future publication.

Figure 3 (top panel) shows the scaled differential cross section $s^7 \frac{d\sigma}{dt}$ as a function of \sqrt{s} for $\theta_{c.m.} = 50^\circ$ to 115° with an angular bin size of 5° for the $\gamma n \rightarrow \pi^- p$ process. As in Fig. 2, the systematic uncertainties are shown as bands in Fig. 3. The arrows indicate the location of \sqrt{s} corresponding to a pion transverse momentum (p_T) of 1.1 GeV/c. This p_T value was suggested to govern the scaling onset by Refs. [9,11]. We note the large discrepancy between our results and those from Ref. [24] at $\theta_{c.m.} = 75^\circ$ and 95° . We also note that the SAID fits [18,19] did not include data from Ref. [24]. An angular-dependent feature in the scaled differential cross section is

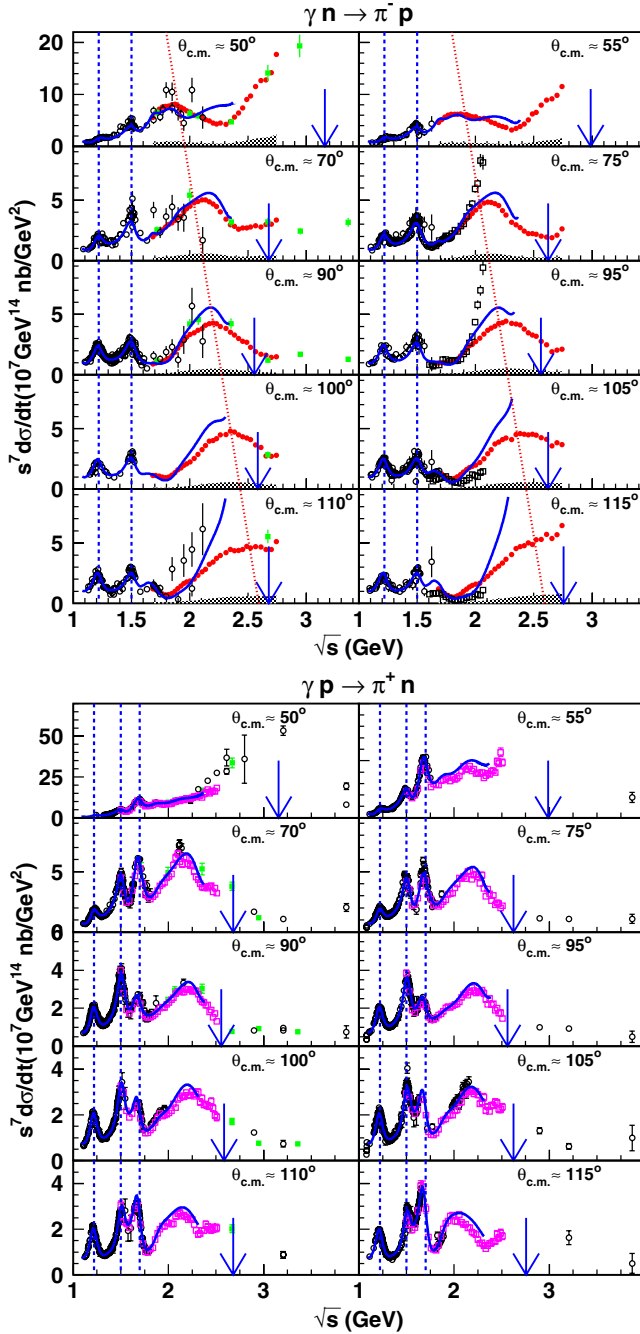


FIG. 3 (color online). Scaled differential cross section $s^7 \frac{d\sigma}{dt}$ for $\gamma n \rightarrow \pi^- p$ (top panel) and $\gamma p \rightarrow \pi^+ n$ (bottom panel) as a function of \sqrt{s} for $\theta_{c.m.} = 50^\circ$ to 115° . The arrows indicate the location of \sqrt{s} corresponding to a transverse momentum value of 1.1 GeV/c. The green solid squares are results from Ref. [1]. The results from this experiment are shown as red solid circles. The magenta open squares are recent CLAS data on π^+ production [19]. The black open circles and open squares are the world data collected from Refs. [5,20] and [24], respectively. Errors on the data from CLAS are the quadratic sum of the statistical and systematic uncertainties. The SAID SP09 results [19] are shown as the blue solid curves. The blue dashed lines indicate the known resonances, and the red dotted lines illustrate the angular-dependent feature of the broad enhancement structure discussed in the text.

clearly seen in our data. The aforementioned broad enhancement around a \sqrt{s} value of 2.1 GeV at $\theta_{c.m.} = 90^\circ$ seems to shift as a function of $\theta_{c.m.}$ from \sqrt{s} of 1.80 GeV at 50° to 2.45 GeV at 105° as shown by the red dotted lines. Our studies show that such behavior is not an artifact of the s^7 scaling factor. It is not clear whether this enhancement dies off for $\theta_{c.m.} > 105^\circ$ or it shifts to further higher energies. The blue dashed lines indicate the locations of the nucleon resonances around 1.2 GeV and 1.5 GeV which, as expected, do not change with $\theta_{c.m.}$. However, such an angular-dependent enhancement is not seen in the π^+ (see the bottom panel of Fig. 3) and π^0 channels from the proton. The SAID FA09 prediction is also shown in Fig. 3 (blue solid curve), and it does show an enhancement around \sqrt{s} of 2.2 GeV which is not angular dependent. Our studies show that such a behavior is not due to the FSI correction. The observed angular-dependent enhancement structure in the π^- channel could be due to some unknown resonances which couple differently to the neutron channel than to the proton channel. Polarization data from all three channels and partial wave analysis are necessary in order to understand the nature of this enhancement and its angular dependence in the π^- channel.

The data presented in this Letter are the first high statistical precision measurement of the differential cross section of the $\gamma n \rightarrow \pi^- p$ process in the region $\sqrt{s} \approx 1.8$ –2.5 GeV with fine photon energy bins, and a pion center-of-mass angle between 50° and 115° . Our data suggest a possible signature for the transition to the CCR scaling region, in the form of a falloff of the scaled cross section over a narrow energy range. An angular-dependent enhancement in the scaled differential cross section has been seen for the first time in our data, which is different from that of the $\gamma p \rightarrow \pi^+ n$ process, and it is also different from the latest SAID prediction.

We acknowledge the outstanding efforts of the staff of the Accelerator and Physics Divisions at Jefferson Laboratory who made this experiment possible. This work was supported in part by the U.S. Department of Energy, the National Science Foundation, the Italian Istituto Nazionale di Fisica Nucleare, the French Centre National de la Recherche Scientifique and Commissariat à l’Energie Atomique, and the Korea Science and Engineering Foundation. Jefferson Science Associates (JSA) operates the Thomas Jefferson National Accelerator Facility for the U.S. Department of Energy under Contract No. DE-AC05-06OR23177.

*Current address: University of Virginia, Charlottesville, Virginia 22901, USA

†Current address: Thomas Jefferson National Accelerator Facility, Newport News, Virginia 23606, USA

‡Current address: The George Washington University, Washington, DC 20052, USA

- [§]Current address: Edinburgh University, Edinburgh EH9 3JZ, United Kingdom
- [1] L. Y. Zhu *et al.*, Phys. Rev. Lett. **91**, 022003 (2003).
[2] L. Y. Zhu *et al.*, Phys. Rev. C **71**, 044603 (2005).
[3] S. J. Brodsky and G. R. Farrar, Phys. Rev. Lett. **31**, 1153 (1973); Phys. Rev. D **11**, 1309 (1975); V. Matveev *et al.*, Lett. Nuovo Cimento Soc. Ital. Fis. **7**, 719 (1973).
[4] G. P. Lepage and S. J. Brodsky, Phys. Rev. D **22**, 2157 (1980).
[5] R. L. Anderson *et al.*, Phys. Rev. D **14**, 679 (1976).
[6] C. White *et al.*, Phys. Rev. D **49**, 58 (1994).
[7] J. Napolitano *et al.*, Phys. Rev. Lett. **61**, 2530 (1988); S. J. Freedman *et al.*, Phys. Rev. C **48**, 1864 (1993); J. E. Belz *et al.*, Phys. Rev. Lett. **74**, 646 (1995).
[8] C. Bochna *et al.*, Phys. Rev. Lett. **81**, 4576 (1998).
[9] E. C. Schulte *et al.*, Phys. Rev. Lett. **87**, 102302 (2001).
[10] M. Mirazita *et al.*, Phys. Rev. C **70**, 014005 (2004).
[11] P. Rossi *et al.*, Phys. Rev. Lett. **94**, 012301 (2005).
[12] B. A. Mecking *et al.*, Nucl. Instrum. Methods Phys. Res., Sect. A **503**, 513 (2003).
[13] D. I. Sober *et al.*, Nucl. Instrum. Methods Phys. Res., Sect. A **440**, 263 (2000).
[14] R. Machleidt, K. Holinde, and C. Elster, Phys. Rep. **149**, 1 (1987).
[15] M. D. Mestayer *et al.*, Nucl. Instrum. Methods Phys. Res., Sect. A **449**, 81 (2000).
[16] H. Gao, R. J. Holt, and V. R. Pandharipande, Phys. Rev. C **54**, 2779 (1996).
[17] J. M. Laget, Phys. Rev. C **73**, 044003 (2006).
[18] M. Dugger *et al.*, Phys. Rev. C **76**, 025211 (2007).
[19] M. Dugger *et al.*, arXiv:0903.1110.
[20] R. A. Arndt, W. J. Briscoe, R. L. Workman, and I. I. Strakovsky, the GWU CNS Database, http://gwdac.phys.gwu.edu/analysis/pr_analysis.html.
[21] S. S. Kamalov *et al.*, Phys. Rev. C **64**, 032201(R) (2001) (a dynamical model); D. Drechsel *et al.*, Nucl. Phys. **A645**, 145 (1999) (a unitary isobar model); D. Drechsel, S. S. Kamalov, and L. Tiator, Eur. Phys. J. A **34**, 69 (2007).
[22] A. Sibirtsev, J. Haidenbauer, S. Krewald, T.-S. H. Lee, U.-G. Meissner, and A. W. Thomas, Eur. Phys. J. A **34**, 49 (2007); A. Sibirtsev (private communications).
[23] C. Amsler *et al.*, Phys. Lett. B **667**, 1 (2008).
[24] H.-J. Besch *et al.*, Z. Phys. C **16**, 1 (1982).